Epitaxial growth and superconductivity of optimally doped $Sr_{1-x}Eu_xCuO_2$ cuprate films

Hang Yan,[1] Ze-Xian Deng,[1] Jia-Qi Fan,[1] Xue-Qing Yu,[1] Xiao-Peng Hu,[1] Can-Li Song,[1,2,*] Xu-Cun Ma,[1,2,†] and Qi-Kun Xue[1,2,3,4]

[1]*State Key Laboratory of Low-Dimensional Quantum Physics, Department of Physics, Tsinghua University, Beijing 100084, China*
[2]*Frontier Science Center for Quantum Information, Beijing 100084, China*
[3]*Beijing Academy of Quantum Information Sciences, Beijing 100193, China*
[4]*Southern University of Science and Technology, Shenzhen 518055, China*

(Received 20 January 2023; revised 29 April 2023; accepted 20 June 2023; published 6 July 2023)

Superconducting infinite-layer $Sr_{1-x}Eu_xCuO_2$ films at optimal doping ($x \sim 0.15$) have been epitaxially grown on $SrTiO_3$(001) substrates with oxide molecular beam epitaxy. By combining x-ray diffraction and transport measurements, we have established a narrow window of growth conditions [i.e., ozone pressure, substrate temperature, (Sr + Eu)/Cu flux ratio, and postannealing] in which the superconducting infinite-layer structure can be readily achieved while eliminating any unwanted competing phases. A smaller out-of-plane lattice constant ($c < 3.42$ Å) is found to be crucial to prompt superconductivity in the $Sr_{1-x}Eu_xCuO_2$ films. Thickness-dependent electrical resistivity measurements reveal superconductivity even when the film thickness is thinned down to 5 nm. Furthermore, the superconducting state of the epitaxial infinite-layer films remains remarkably stable against air exposure, providing an ideal platform to explore the high-temperature superconductivity and unusual properties in cuprates.

DOI: 10.1103/PhysRevMaterials.7.074802

I. INTRODUCTION

Infinite-layer (IL) $ACuO_2$ (A = Ca, Sr, Ba) compounds have the simplest crystal structure of all cuprate superconductors, where the superconducting CuO_2^{2-} layer and A^{2+} ionic layer as charge reservoirs are stacked alternately along the c-axis direction [1–4]. Superconductivity arises upon appropriate electron doping by partial replacement of A^{2+} by trivalent ions of lanthanides, with the highest transition temperature (T_c) of 43 K previously reported in $Sr_{1-x}La_xCuO_2$ [5]. More importantly, it was evident that the IL cuprates are uniquely terminated by the quintessential superconducting CuO_2 planes [6–8], which contrast markedly with other cuprate superconductors that are often terminated by the charge reservoir layers, e.g., BiO for the bismuth-based cuprates [9–11]. Therefore, the IL cuprates naturally serve as an ideal system to explore directly the electronic structure of CuO_2 planes and are beneficial to understand the microscopic mechanism of high-T_c superconductivity in cuprates [12,13]. Actually, the robust Mott-Hubbard band structure against ambipolar chemical doping, nodeless superconductivity, and lattice vibrations have been experimentally observed on CuO_2 that challenge unconventional wisdom of the cuprate superconductors [14–17]. Unfortunately, the available research on metastable IL cuprates is largely constrained by the difficulty of high-quality single-crystalline material synthesis [18–20], especially their close proximity to competing Sr-Cu-O compounds of Sr_2CuO_3, $Sr_{14}Cu_{24}O_{41}$, and orthorhombic $SrCuO_2$ [21–24]. The situation becomes even worse by the limited solubility of lanthanides explored before, which has imposed severe restrictions on the available electron doping range [20,25].

Efforts on epitaxial growth of IL cuprate films on $SrTiO_3$(001) substrates by ozone-assisted molecular beam epitaxy (OMBE) have recently led to the successful preparation of $Sr_{1-x}Eu_xCuO_2$ (SECO) superconducting samples over a wide doping range (x up to 0.25), in which percolative superconductivity has been identified [26]. Compared to the previously explored lanthanum and neodymium dopants, the lanthanide europium has a smaller ionic radius (0.947 Å) and more effectively reduces the in-plane lattice constant mismatch (∼1.1%) between the $SrTiO_3$ (3.905 Å) and SECO (∼3.95 Å) thin films that thus benefit the emergence of superconductivity [27]. In this work, we combine x-ray diffraction (XRD) and electrical transport measurements to systematically investigate OMBE-grown SECO films at the optimal doping ($x \sim 0.15$), which enables us to establish the epitaxial growth recipe for optimal superconductivity in IL cuprate films. At a fixed ozone pressure, the (Sr + Eu)/Cu flux ratio and postannealing are revealed to be essentially important to access the superconducting single-crystalline SECO films, in which Laue fringes and a step-terrace surface are apparently observed. Furthermore, we find that the superconductivity is sustained in SECO films, even at a thickness of 5 nm, and is highly stable against air exposure.

II. METHODS

Our experiments were carried out in a homemade OMBE system, integrated with an ozone gas delivery system. Semi-insulating $SrTiO_3$(001) substrates with ∼0.05 wt% niobium dopants were first degassed at 600 °C overnight and then annealed at 1200 °C for 20 minutes to obtain an atomically flat surface. Prior to SECO film epitaxy, fluxes of high-purity

*Corresponding author: clsong07@mail.tsinghua.edu.cn
†Corresponding author: xucunma@mail.tsinghua.edu.cn

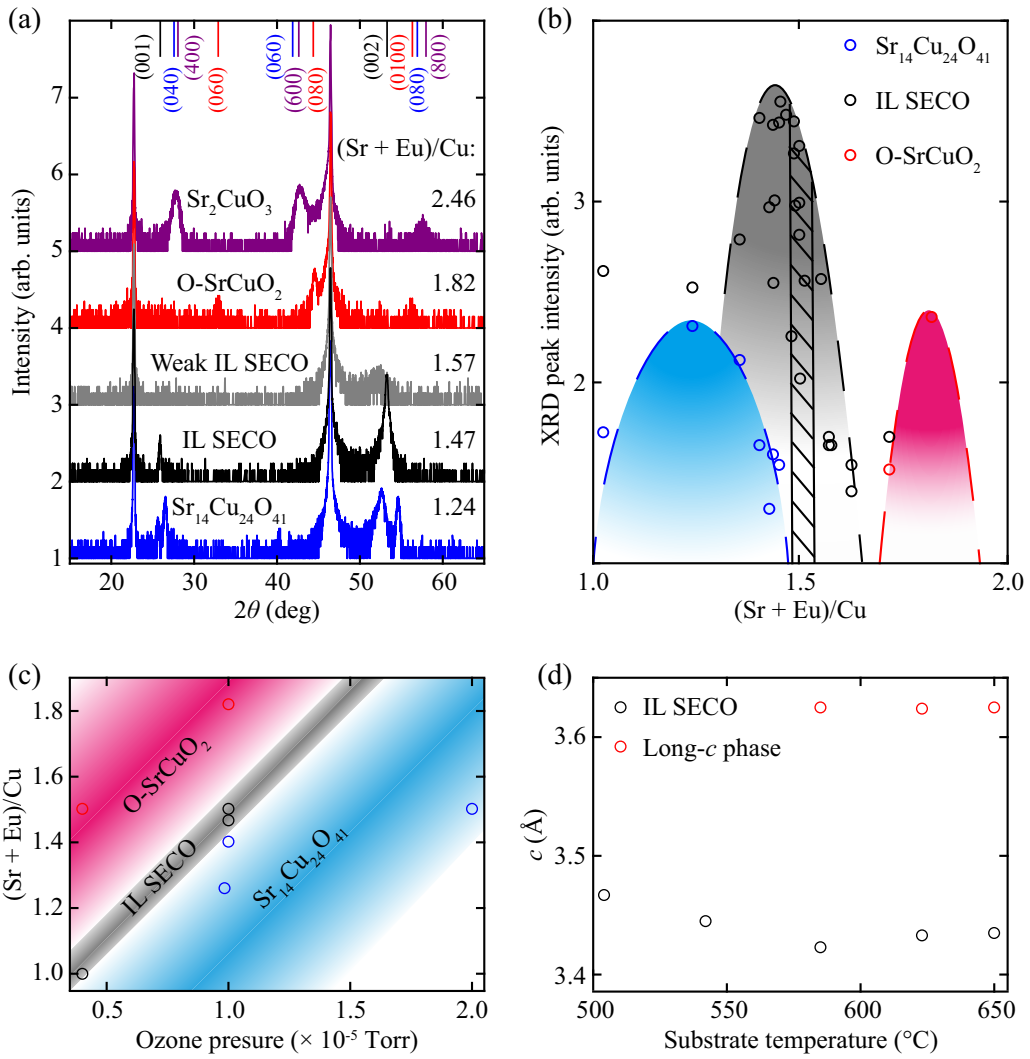

FIG. 1. (a) XRD θ-2θ patterns of epitaxial SECO films grown with various flux ratios of (Sr + Eu)/Cu as indicated. (b) XRD intensity of various Sr(Eu)-Cu-O phases as a function of the (Sr + Eu)/Cu flux ratio. (c) (Sr + Eu)/Cu flux ratio-ozone pressure phase diagram of the Sr-(Eu)-Cu-O system. (d) Substrate temperature dependence of out-of-plane lattice constant c for both the IL SECO and long-c phases.

copper (99.9999%), strontium (99.95%), and europium (99.9%) metal sources are finely calibrated in sequence by using a standard quartz crystal microbalance (Inficon SQM160H). Epitaxial SECO thin films were subsequently prepared by codeposition of all metal sources under desired ozone beams, monitored by time-resolved reflection high-energy electron diffraction (RHEED). The growth rate of SECO films was typically 5.5 Å per minute. After postannealing treatment in an ultra-high vacuum (UHV), the samples were transferred out of the UHV chamber for *ex situ* XRD measurements using monochromatic copper $K_{\alpha 1}$ radiation with a wavelength of 1.5406 Å. The resistivity measurements were conducted on a standard physical property measurement system (Quantum Design) via a four-terminal configuration.

III. RESULTS

Provided many competing phases in the Sr(Eu)-Cu-O system, we started with an analysis of the major role of the nominal flux ratio of Sr + Eu and Cu sources during the epitaxial growth. Figure 1(a) depicts the representative XRD patterns of the epitaxial SECO films with different (Sr + Eu)/Cu flux ratios at a fixed ozone pressure of 1.0×10^{-5} Torr and a substrate temperature of 540 °C. One can immediately see that the high-quality SECO thin films with a pure IL structure are formed in an intermediate (Sr + Eu)/Cu flux ratio of ∼1.47. Otherwise, the orthorhombic $SrCuO_2$ (O-$SrCuO_2$) and Sr_2CuO_3 develop at a higher flux ratio, while the spin ladder $Sr_{14}Cu_{24}O_{41}$ dominates at a lower flux ratio (∼1.24). In addition, we observe that the XRD intensity of the IL $SrCuO_2$ peak is significantly suppressed when the (Sr + Eu)/Cu flux ratio changes slightly by 0.1, hinting at an extremely narrow window for the epitaxial growth of high-quality, single-phase IL SECO films. This can be seen more clearly in Fig. 1(b), where we have shown the XRD intensities for various competing phases as a function of the (Sr + Eu)/Cu flux ratio. The high-quality and single-phase IL SECO films can only be realized in a narrow window (∼0.1) of the (Sr + Eu)/Cu flux ratio.

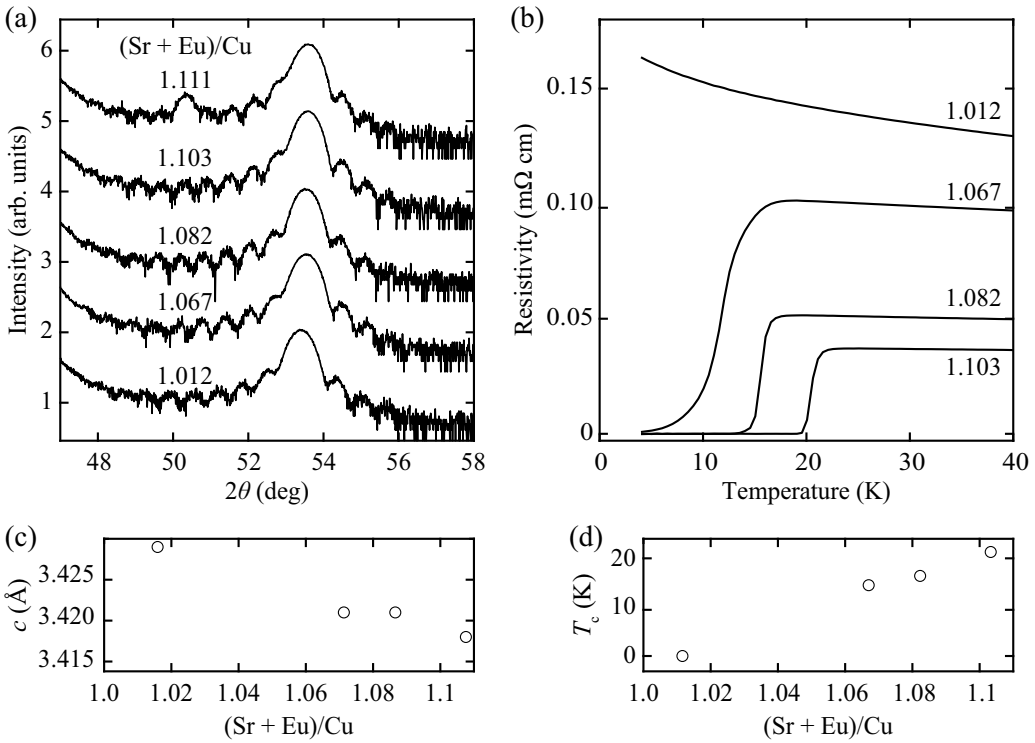

FIG. 2. (a) XRD patterns around the (002) diffraction peaks of the SECO films grown with different (Sr + Eu)/Cu flux ratios. (b) Electrical resistivity as a function of temperature for the SECO films grown with various (Sr + Eu)/Cu flux ratios. (c) (Sr + Eu)/Cu flux ratio dependence of the lattice constant c. (d) (Sr + Eu)/Cu flux ratio dependence of T_c.

The ozone pressure and substrate temperature have also imposed significant influences on the epitaxial growth of IL SECO films. In Fig. 1(c), we extract the phase diagram of the Sr(Eu)-Cu-O system versus the ozone pressure and the (Sr + Eu)/Cu flux ratio. It appears that the suitable flux ratio for epitaxial IL SECO (also for the other phases) increases as the ozone pressure is elevated, which should arise from the reduction in the strontium and europium flux due to their easy oxidization on the way depositing onto the substrates [28]. Furthermore, we find that as the growth temperature increases to 580 °C [Fig. 1(d)], another phase with an extended out-of-plane lattice constant c, often called the long-c phase, develops and coexists with the IL SECO films, which is caused by the excess oxygens occupying the apical positions of the copper atoms [5,15,29]. To avoid this unwanted long-c phase, we thereafter fix the ozone pressure and substrate temperature at 4×10^{-6} Torr and 540 °C, respectively, in which the IL SECO epitaxial films are formed in a flux ratio of about 1.0 [Fig. 1(c)].

Having achieved the single-phase IL SECO epitaxial films, we find that not all samples are superconducting. In order to improve the film quality further and access superconductivity, we have to tune more finely the (Sr + Eu)/Cu flux ratio in the narrow growth window of the IL structure. Figures 2(a) and 2(b) show several representative XRD spectra and the electrical resistivity-temperature curves of the SECO films at varied (Sr + Eu)/Cu flux ratios, all of which were postannealed at a growth temperature of 540 °C for 60 minutes. It is evident that a tiny change in the flux ratio (∼0.01) can profoundly alter the lattice constant and T_c [Figs. 2(c) and 2(d)]. By increasing the (Sr + Eu)/Cu flux ratio from 1.012 to 1.111, the position of the (002) diffraction peak of IL SECO films gradually shifts toward the higher angles of 2θ; that is, the c-axis lattice constant gets smaller from 3.429 Å to 3.418 Å. At the same time, the Laue fringes around the (002) diffraction peaks become clearer, which means higher crystalline quality of the IL SECO films. As a result, the electrical resistivity-temperature curves change from an insulating behavior at a lower (Sr + Eu)/Cu flux ratio (∼1.012) to superconducting ones at a higher flux ratio (>1.067). As the (Sr + Eu)/Cu flux ratio increases more, the superconducting state displays higher T_c, which can be as high as 21.3 K [Figs. 2(b) and 2(d)]. If we further increase the (Sr + Eu)/Cu flux ratio, the long-c phase starts to appear and increases in concentration with an increasing (Sr + Eu)/Cu flux ratio, the underlying mechanism of which is subject to further investigation. In any case, our experiments suggest that the (Sr + Eu)/Cu flux ratio is quite narrow for the epitaxial growth of high-quality, superconducting IL SECO films.

It should be emphasized that all the as-grown IL SECO samples exhibit a relatively large (>3.420 Å) c-axis lattice constant due to the presence of excess apical oxygens that are generally detrimental to superconductivity. To eliminate the apical oxygens, an extra reduction after annealing in the UHV is routinely needed to realize the superconducting state [3,4,30]. We have thus prepared IL SECO samples under identical conditions [ozone pressure, substrate temperature, (Sr + Eu)/Cu flux ratio of ∼1.08], but annealed them at 540 °C for various durations, ranging from 0 to 120 minutes, as shown in Fig. 3. As a consequence of the optimal (Sr + Eu)/Cu flux ratio that we used, clear Laue fringes [Fig. 3(a)] and a superconducting transition [Fig. 3(b)] can be

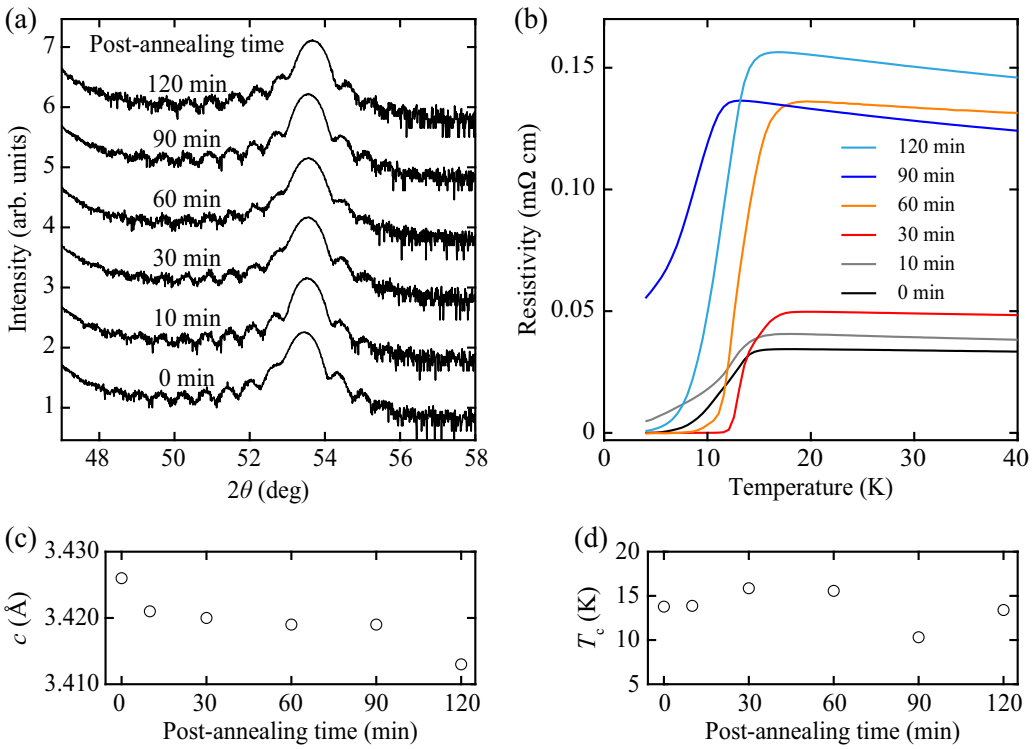

FIG. 3. (a) XRD patterns around the (002) diffraction peaks of the SECO films after different postannealing times. (b) Resistivity ρ(T) as a function of the temperature for SECO films with different postannealing times. (c) Postannealing time dependence of the lattice constant c. (d) Postannealing time dependence of T_c.

invariably observed in all the SECO epitaxial films. However, the SECO (002) diffraction peak moves toward higher angles of 2θ with extended postannealing time; that is, the c-axis lattice constant decreases from 3.426 Å for the as-grown sample to 3.413 Å for the sample annealed for 120 minutes [Fig. 3(c)]. The reduced c-axis lattice constant strongly shows the removal of excess apical oxygens upon postannealing, which considerably affects the electrical transport behaviors shown in Figs. 3(b) and 3(d). For the as-grown sample and the sample annealed for 10 minutes only, the superconducting transition is very broad, with a T_c of ∼13.7 K, and the resistivity is finite even down to 4 K. As the postannealing time increases to 30 to 60 minutes, the superconductivity is obviously enhanced, with a sharp superconducting transition and zero-resistance states below $T_c \sim 15.7$ K. As the postannealing time is further prolonged, however, the superconductivity gets weaker. This implies that a moderate postannealing time of ∼30 to 60 minutes is required to obtain high-quality IL cuprate films with optimal superconductivity.

Next we investigate the thickness dependence of superconductivity for IL SECO cuprate films, given that the film thickness usually serves as a key factor in determining the unusual properties of superconductors [31,32]. According to the well-established growth recipes noted earlier, we have prepared a series of SECO samples with different film thicknesses by finely controlling the (Sr + Eu)/Cu flux ratio (∼1.08), substrate temperature (540 °C), and postannealing time (30 minutes), and by adjusting the growth time under an identical deposition rate (∼5.5 Å/minute). The estimated film thicknesses, ranging from 2.5 nm to 33.6 nm, match quite nicely with the calculated ones from the Laue fringes around the SECO (002) diffraction peaks in Fig. 4(a). One can see that, except for the SECO sample with a thickness of only 2.5 nm, where the spacing of the Laue fringes is too large to be recognized, the Laue fringes are clearly observable in other samples. Regardless of the film thickness, all IL SECO samples are characteristic of a regular step-terrace surface, as confirmed by our atomic force microscopy (AFM) images in Fig. 4(b). This hints at a step-flow growth mode of the IL SECO films on $SrTiO_3$(001) substrates [33], which matches nicely with our RHEED measurements, presenting no obvious intensity oscillations. In Figs. 4(c) and 4(d), we show the electrical resistivity-temperature curves of the IL SECO films, which reveal an apparent thickness dependence. Except for the thinnest and insulating sample with a thickness of only 2.5 nm, other IL SECO films are superconducting with smaller normal-state resistivity. Importantly, the sharp superconducting transition can be achieved in IL SECO films with a thickness of only 5 nm. As far as we know, this is the thinnest superconducting IL cuprate film. Compared to the 16.4-nm film, the thickest SECO film of ∼33.6 nm exhibits relatively large resistivity in the normal state, possibly owing to the film thickness-dependent epitaxial strain.

Last, we comment on the air stability of the superconducting IL SECO films. Figure 5(a) compares the XRD spectra of one identical SECO film (∼16 nm) measured just after growth and after 110 days without a protective coating. Although in the metastable IL phase, no obvious changes can be observed in both the diffraction peaks and the corresponding intensities, indicating highly air-stable IL epitaxial films

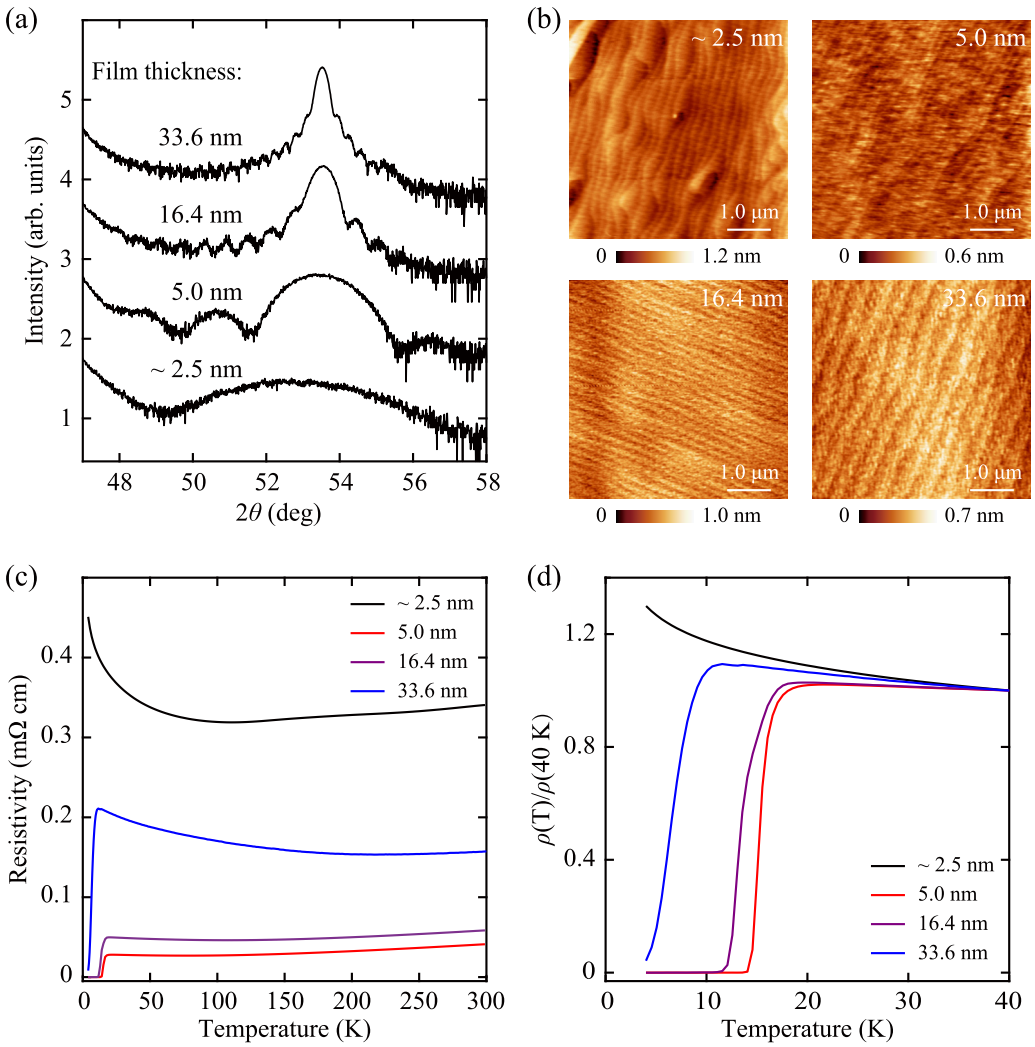

FIG. 4. (a) XRD patterns around the (002) diffraction peaks of the SECO films with different film thicknesses. (b) AFM images (5 μm × 5 μm) of SECO films showing a regular step-terrace morphology, regardless of the IL SECO film thickness. (c) and (d) Electrical resistivity and corresponding normalized resistivity $\rho(T)/\rho(40\ K)$ as a function of the temperature for SECO films with different film thicknesses, respectively.

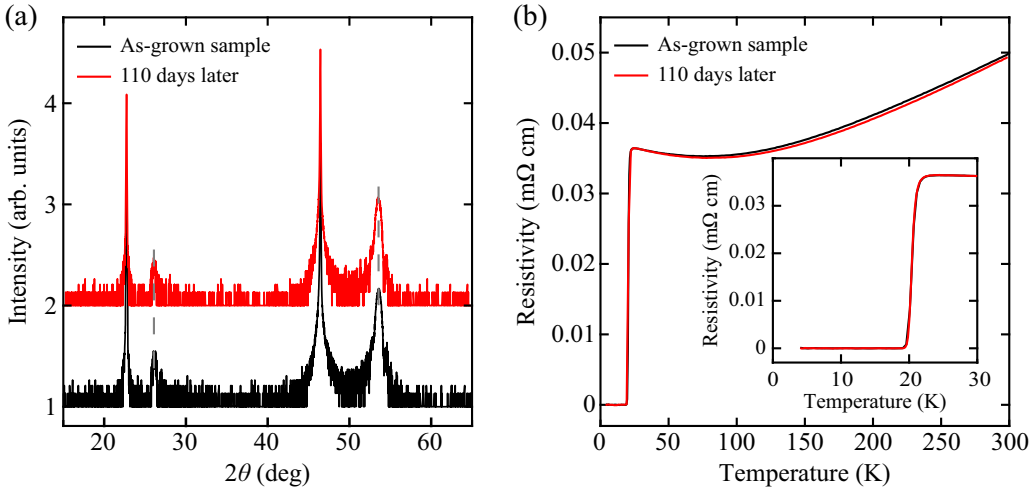

FIG. 5. (a) XRD patterns of one as-grown SECO film (black lines) and 110 days later after growth (red lines). The dashed gray lines represent locations of XRD peaks for the IL SECO phase. (b) Electrical resistivity as a function of the temperature for the corresponding SECO film in (a). The inset shows the same $\rho(T)$ curves in a narrow temperature region (4 K to 30 K).

on the $SrTiO_3$(001) substrates. This has been further convincingly confirmed by the electrical transport measurements in Fig. 5(b). After more than three months, the electrical resistivity-temperature curve can nicely collapse onto the previous one, especially around the superconducting transition region [see the inset in Fig. 5(b)], with the same critical temperature T_c [Fig. 5(b)].

IV. CONCLUSION

In summary, we have succeeded in preparing IL SECO films at optimal doping on $SrTiO_3$ substrates using the state-of-the-art OMBE technique, and performed systematic XRD and electrical transport measurements. This allows us to establish the growth-phase diagram, based on which one can readily grow single-phase, superconducting IL SECO films in a narrow window of growth conditions. We reveal that the precise control of ozone pressure, substrate temperature, (Sr + Eu)/Cu flux ratio, and postannealing time are all crucial for realizing the superconductivity of SECO films. The growth recipes established here, together with the robust superconductivity against film thickness and air exposure, render epitaxial IL films an alternative prototype for more systematic investigations of the electronic structure and superconductivity in cuprates.

ACKNOWLEDGMENT

The work was financially supported by the National Key R&D Program of China (Grant No. 2022YFA1403100) and the National Natural Science Foundation of China (Grant No. 12134008).

[1] T. Siegrist, S. M. Zahurak, D. W. Murphy, and R. S. Roth, Nature (London) **334**, 231 (1988).
[2] M. G. Smith, A. Manthiram, J. Zhou, J. B. Goodenough, and J. T. Markert, Nature (London) **351**, 549 (1991).
[3] N. P. Armitage, P. Fournier, and R. L. Greene, Rev. Mod. Phys. **82**, 2421 (2010).
[4] P. Fournier, Physica C **514**, 314 (2015).
[5] S. Karimoto, K. Ueda, M. Naito, and T. Imai, Appl. Phys. Lett. **79**, 2767 (2001).
[6] K. Koguchi, T. Matsumoto, and T. Kawai, Science **267**, 71 (1995).
[7] J. W. Harter, L. Maritato, D. E. Shai, E. J. Monkman, Y. Nie, D. G. Schlom, and K. M. Shen, Phys. Rev. B **92**, 035149 (2015).
[8] Y. Zhong, S. Han, Y. Wang, Z. Luo, D. Zhang, L. Wang, W. Li, K. He, C. L. Song, X. C. Ma, and Q. K. Xue, Phys. Rev. B **97**, 245420 (2018).
[9] Ø. Fischer, M. Kugler, I. Maggio-Aprile, C. Berthod, and C. Renner, Rev. Mod. Phys. **79**, 353 (2007).
[10] S. H. Pan, J. P. O'Neal, R. L. Badzey, C. Chamon, H. Ding, J. R. Engelbrecht, Z. Wang, H. Eisaki, S. Uchida, A. K. Gupta, K. W. Ng, E. W. Hudson, K. M. Lang, and J. C. Davis, Nature (London) **413**, 282 (2001).
[11] Y. F. Lv, W. L. Wang, J. P. Peng, H. Ding, Y. Wang, L. Wang, K. He, S. H. Ji, R. Zhong, J. Schneeloch, G. D. Gu, C. L. Song, X. C. Ma, and Q. K. Xue, Phys. Rev. Lett. **115**, 237002 (2015).
[12] P. A. Lee, N. Nagaosa, and X. G. Wen, Rev. Mod. Phys. **78**, 17 (2006).
[13] B. Keimer, S. A. Kivelson, M. R. Norman, S. Uchida, and J. Zaanen, Nature (London) **518**, 179 (2015).
[14] J. W. Harter, L. Maritato, D. E. Shai, E. J. Monkman, Y. Nie, D. G. Schlom, and K. M. Shen, Phys. Rev. Lett. **109**, 267001 (2012).
[15] Y. Zhong, J. Q. Fan, R. F. Wang, S. Wang, X. Zhang, Y. Zhu, Z. Dou, X. Q. Yu, Y. Wang, D. Zhang, J. Zhu, C. L. Song, X. C. Ma, and Q. K. Xue, Phys. Rev. Lett. **125**, 077002 (2020).
[16] R. F. Wang, J. Guan, Y. L. Xiong, X. F. Zhang, J. Q. Fan, J. Zhu, C. L. Song, X. C. Ma, and Q. K. Xue, Phys. Rev. B **102**, 100508(R) (2020).
[17] J. Q. Fan, X. Q. Yu, F. J. Cheng, H. Wang, R. Wang, X. Ma, X. P. Hu, D. Zhang, X. C. Ma, Q. K. Xue, and C. L. Song, Natl. Sci. Rev. **9**, nwab225 (2022).
[18] M. Takano, Y. Takeda, H. Okada, M. Miyamoto, and T. Kusaka, Physica C **159**, 375 (1989).
[19] G. Er, S. Kikkawa, and F. Kanamaru, Physica C **235-240**, 983 (1994).
[20] N. Ikeda, Z. Hiroi, M. Azuma, M. Takano, Y. Bando, and Y. Takeda, Physica C **210**, 367 (1993).
[21] Y. Krockenberger, K. Sakuma, and H. Yamamoto, Appl. Phys. Express **5**, 043101 (2012).
[22] Y. Krockenberger, A. Ikeda, K. Kumakura, and H. Yamamoto, J. Appl. Phys. **124**, 073905 (2018).
[23] J. Q. Fan, S. Z. Wang, X. Q. Yu, R. F. Wang, Y. L. Xiong, C. L. Song, X. C. Ma, and Q. K. Xue, Phys. Rev. B **101**, 180508(R) (2020).
[24] Z. Chen, Y. Wang, S. N. Rebec, T. Jia, M. Hashimoto, D. Lu, B. Moritz, R. G. Moore, T. P. Devereaux, and Z. X. Shen, Science **373**, 1235 (2021).
[25] A. Ikeda, Y. Krockenberger, and H. Yamamoto, Phys. Rev. Mater. **3**, 064803 (2019).
[26] X. Q. Yu, H. Yan, L. X. Wei, Z. X. Deng, Y. L. Xiong, J. Q. Fan, P. Yu, X. C. Ma, Q. K. Xue, and C. L. Song, Phys. Rev. B **106**, L100503 (2022).
[27] S. Karimoto and M. Naito, Physica C **412**, 1349 (2004).
[28] E. S. Hellman and E. H. Hartford, J Vac. Sci. Technol. B **12**, 1178 (1994).
[29] V. Leca, D. H. A. Blank, G. Rijnders, S. Bals, and G. van Tendeloo, Appl. Phys. Lett. **89**, 092504 (2006).
[30] L. Maritato, A. Galdi, P. Orgiani, J. W. Harter, J. Schubert, K. M. Shen, and D. G. Schlom, J. Appl. Phys. **113**, 053911 (2013).
[31] Q. Y. Wang, Z. Li, W. H. Zhang, Z. C. Zhang, J. S. Zhang, W. Li, H. Ding, Y. B. Ou, P. Deng, K. Chang, J. Wen, C. L. Song, K. He, J. F. Jia, S. H. Ji, Y. Y. Wang, L. L. Wang, X. Chen, X. C. Ma, and Q. K. Xue, Chin. Phys. Lett. **29**, 037402 (2012).
[32] D. Qiu, C. Gong, S. Wang, M. Zhang, C. Yang, X. Wang, and J. Xiong, Adv. Mater. **33**, 2006124 (2021).
[33] J. Choi, C. B. Eom, G. Rijnders, H. Rogalla, and D. H. A. Blank, Appl. Phys. Lett. **79**, 1447 (2001).